# MULTI-SYSTEM COUPLING VIBRATION OF A DISTRIBUTED ELECTRIC-DRIVE AGRICULTUAL VEHICLE
# /
# 分布式电传动农用汽车多系统耦合振动研究

**Ph.D. Jin C.[1)], Ms. Wei J.[1)], Ph.D. Stud. Sun H.[1)], Ph.D Stud Yin Y.[2)]**
[1)]School of Mechanical Engineering, University of Science and Technology Beijing, Beijing / China,
[2)] Department of Mechanical and Industrial Engineering, Concordia University / Canada
*Tel:010-82375949; E-mail: jinjinbit@163.com*

***Abstract:*** *To ensure riding comfort, vibration generated by engine, drive system and ground need to be considered in designing an agricultural vehicle. This study examines multi-body dynamics model of an agricultural vehicle, and focuses on the distributed electric-drive agricultural vehicle. To simulate the response of an electric-drive agricultural vehicle to vibrations excited by the drive motors, engine and road roughness, this study proposes a vibration model of a distributed electric-drive agricultural vehicle that has 11 degrees of freedom and coupled excitation sources. The model was derived from vehicle dynamics equations and solved numerically employing fast Fourier transform. The model was validated in experiments on a real distributed electric-drive agricultural vehicle. Simulations and experiments showed that the amplitude of low-frequency vibration of the cab was increased by simultaneous excitations, which could not be ignored. This result is useful for the design of the suspension component and overall design of agricultural machinery.*

***Keywords:*** *Electric drive; Agricultural vehicle; Riding comfort; Vibrations; Multiple systems*

## INTRODUCTION

An electric-drive agricultural vehicle is energetically efficient, environmentally friendly and convenient. It is increasingly being used for transportation work in farm lands. However, because of road roughness, simultaneous shocks generated by farming land and vehicle systems have a significant effect on the health of the driver and the reliability of the vehicle. A distributed electric-drive agricultural vehicle is powered by hybrid of diesel engine and battery. Compared with the traditional mechanical transmission, the vehicle is specially designed for farming lands with in-motor wheel, and deleting the gearbox, driveshaft, final drive, differential, so the vehicle has advantages of simple structure, small space requirement, easy high torque performing, convenient feedback control and continuous speed change. Thus, the wheel electric drive has great application potential for agricultural vehicles. However, an electric-drive agricultural vehicle has a significant unsprung load. Additionally, the connection of the hydro-pneumatic spring and wheel rim drive unit generates interacting vibrations from the engine and drive motor and reduces the ride comfort. Thus, the relationship between ride comfort and the structure of the distributed electric-drive agricultural vehicle should be examined.

Present studies on the effects of drive motor vibration on vehicle power and riding comfort usually focus on passenger cars, and the drive motor is typically designed as a sprung load [1,5,7,14,17]. Researchers have analyzed the vibration of a switched reluctance

***摘要：****为确保行驶平顺性，农用汽车设计需综合考虑动力、传动系统及地面冲击产生的振动。论文以分布式电传动农用汽车为研究对象，提出了十一自由度发动机激振—电动机激振—路面不平度耦合振动模型。推导出整机动力学方程，并利用快速傅立叶变换方法得到了数值计算结果。通过实车试验与耦合振动模型进行对比，结果表明在考虑驱动电机及发动机激振影响下驾驶室振动的低频段振幅明显增大，在发动机及驱动电机激振力频率段影响明显，不可忽略。通过分析实测数据验证了耦合激励模型在实车中的有效性.耦合激励模型对农用汽车悬架及整车平顺性设计具有指导意义。*

***关键词：****电驱动；农用汽车；平顺性；振动；多系统*

## 引言

电传动农用汽车具有节能、环保、便捷等优势，目前，在农耕地上承担越来越多的运输及装卸工作。但是，农业耕地属于非公路，其路面不平度产生的冲击和车辆本身的振动对驾驶员的健康及车辆的可靠性有很大影响。分布式电传动农用汽车动力系统采用柴油机与蓄电池混合动力。其传动方式不同于传统的机械传动，牵引电动机直接驱动车轮，省去了变速箱、传动轴、主减速器、差速器等传动部件，牵引力大、结构简单、可靠性高，同时便于实现反馈控制和无级变速平稳运行，具有良好的应用前景。但是，该传动方式以轮边驱动单元作为驱动桥，非簧载质量大，悬架下端与轮边驱动单元相连接，牵引电动机与发动机共同作为激振源引起车辆平顺性恶化。因此，对分布式电传动结构形式带来的整车平顺性问题的研究是十分有必要的。

牵引电动机振动对车辆动力性及平顺性能的影响，目前研究多集中于乘用车[1,5,7,14,17]。有学者以开关磁阻驱动电机的振动为例分析，表明电机激振力对悬架系统的影响较大而不能忽略[9]；谭迪以 1/4 车辆简化模型探讨非簧载质量增加对平顺性影响[12]；李朝峰等针对四轮乘用车

motor and pointed out that the effect of motor excitation on the suspension cannot be ignored [9]. Tan [12] built a ¼ vehicle model and discussed the effect of increasing the unsprung load on the riding comfort. Li, using road excitation as the main source of motivation, established a nonlinear model of riding comfort with 11 degrees of freedom (DOFs) for a passenger car [6]. The analysis of riding comfort by Wellman and Wang showed that the powertrain and road excitation cannot be ignored [15, 16]. However, few studies on riding comfort have investigated the coupled excitation effects of the in-wheel motor, engine and road for a distributed electric-drive agricultural vehicle. This paper initiates modeling and discussion on this topic.

Taking the distributed electric-drive agricultural vehicle as the study object, this paper proposes a method of describing the coupled vibration generated by multiple systems of the vehicle and builds a vibration model with 11 DOFs. Moreover, the riding comfort of the vehicle travelling on random surfaces is simulated by employing white-noise filtering. The model and simulation are validated in experiments on a real vehicle undergoing coupled vibration.

建立了 11 自由度非线性车辆平顺性模型，模型主要取路面激励为主要的激励来源[6]；Wellman Thomas 和王登峰针对动力总成振动对整车行驶平顺性展开分析，表明动力总成和路面激励在平顺性分析中不可忽略[15,16]。分析常见车辆平顺性研究，以分布式电驱动车辆为研究对象的论文较少，激励源往往没有同时考虑驱动电机激励、发动机激振、路面不平度的影响，本文正是基于以上问题展开建模和讨论。

本文以分布式电驱动农用汽车为研究对象，提出了兼顾电机激振、发动机振动路面不平度来描述整车多系统耦合运动的方法，建立整车十一自由度的振动模型。采用白噪声滤波法模拟时域内的随机路面进行平顺性仿真。通过联立运动方程分析振动特性并进行了实车现场测试，探究在耦合激励下整车平顺性的影响。

## MATERIALS AND METHODS

## 材料与方法

### *Vibration subsystem analysis of the electric-drive agricultural vehicle*

### *分布式电驱动农用汽车振动子系统分析*

An engine vibration system has a variety of vibration forms. The dominant vibration is the oscillation of the whole machinery, which is much stronger than the vibration of an axle or local vibration [2].

As mentioned, the road roughness, engine vibration and in-wheel electric motor vibration are excitation sources of vibration. The vibration subsystem includes the engine vibration system and in-wheel electric motor vibration system. The electric-drive agricultural vehicle studied in this paper has a Cummings engine. The vibration of the engine is mainly due to the unbalanced forces and torques produced in operating the engine. According to the characteristics of the engine, the excitation frequency is [4]:

发动机系统运转时，机体上存在各种激振力。产生的整机振动主要指机体跳动，这类振动对机体的结构影响较大,而轴系振动、局部振动影响较小[2]。

如前所述，系统振动的激励源包括：路面不平度，发动机振动以及轮边电机振动激励。整机振动子系统包括发动机振动系统和轮边电机振动系统。本文所研究的分布式电驱动农用汽车采用康明斯发动机，发动机振动主要来自于发动机运转过程中产生的不平衡力和力矩，根据发动机自身的工作特性可知，发动机的激励频率为 [4]：

$$f = \frac{n\lambda Z}{60\tau} \tag{1}$$

Where, $\tau$—the stroke number, $n$—the engine speed (r/min), $Z$—the cylinder number, and $\lambda$—the incentive order.

The engine exciting force is mainly generated by the imbalance torque and moment produced by the running of the engine. According to the working characteristics of the four-cylinder engine, a cycle of crank shaft rotation has two instances of torque fluctuation. Based on the traditional dynamic analysis formula, two reciprocating inertia force expressions are [18]:

式中：$\tau$—冲程数，$n$—发动机转速（r/min），$Z$—气缸数，λ—激励阶数。

发动机激振力主要来自于发动机运转过程中产生的不平衡力和力矩根据发动机自身的工作特性可知：在四缸发动机中曲轴每转一周就会产生两次转矩波动。按照传统的动力学分析公式 二次往复惯性力表达式为[18]：

$$P_j = -4\lambda m_j r w^2 \cos(2\alpha) = -4\lambda m_j r w^2 \cos(wt + \varphi) \tag{2}$$

$$m_j = m_{hz} + m_A \tag{3}$$

Where, $P_j$—twice the reciprocating inertia force, $\lambda$—the link ratio, $r$—the radius of the crank, $m_{hz}$—the quality of the piston assembly, and $m_A$—the quality of the small end of the link.

In the experiment conducted in this study, the engine speed measured using a controller area network was

式中：$P_j$—二次往复惯性力；$\lambda$—连杆比；$r$—曲柄半径；$m_{hz}$—活塞组件的质量，$m_A$—双质量系统代换得到的连杆小头的质量。

1500 rpm when the vehicle speed reached 30 km/h. Using equation (1), we calculated the first-order excitation frequency of the engine as 37.5 Hz and the force as 25.3 kN. These results are consistent with data provided by the engine manufacturer.

The drive motor vibration comprises electromagnetic vibration, mechanical vibration and pneumatic vibration [3]. The electromagnetic vibration is generated by the interaction of the magnetic field in the air gap, and varies with time and space. It is also a major vibration source [8]. The main frequency of the drive motor is twice the power frequency. For a synchronous motor, the relation between the revolving speed and power frequency is) [11]:

后续试验过程中车速为 30km/h 时，CAN 数据采得发动机转速 n 为 1500 r/min，代入式（1）可得理论的发动机一阶激励频率为 37.5Hz，采得大小为 25.3kN，这与发动机厂家提供数据一致。

对于电动机系统振动分别由电磁振动、机械振动、气体振动三部分组成[3]。电磁振动是由气隙中磁场的相互作用而产生，且随时间和空间变化，电磁振动为主要振动源[8]。电动机振动力主波频率为二倍电源频率。对于同步电机，转速与供电电源频率关系如下[11]：

$$n' = \frac{60f'}{p} \tag{4}$$

Where, *f'*—the power frequency, *p*—the number of drive motor pole pairs, *n'*—the drive motor speed (r/min).

The Maxwell stress tensor is used to calculate the electromagnetic exciting force acting on the stator. Here, the magnetic field strength on the surface of the strain object is H, the object is surrounded by air and the electromagnetic force acting on the object is[10]:

式中：*f'*—供电频率；*p*—电动机极对数；*n'*—电动机转速（r/min）。

定子上受到的电磁激振力可用麦克斯韦应力张量法计算，假设受力物体表面 S 上的磁场强度为 H，并且这个物体外部被空气所包围，则这个物体受到的电磁力[10]为：

$$\hat{F} = \int_s \left[ -\frac{\mu_0}{2} H^2 \hat{n} + \mu_0 \left( \hat{n} \cdot \hat{H} \right) \hat{H} \right] ds \tag{5}$$

The force can be decomposed into x (vertical) and y (horizontal) directions:

将力分解在 x（垂直）和 y（水平）方向，则:

$$F_x = \int_s \mu_o H_x H_y ds \tag{6}$$

$$F_y = \int_s \frac{\mu_o}{2} (H_y^2 - H_x^2) ds \tag{7}$$

Where, $\mu_0$—the permeability of air, *n*—a unit vector normal to the surface S, and $\boldsymbol{H_x}$ and $\boldsymbol{H_y}$ are the magnetic strength in the *x* and *y* directions respectively. The magnetic field distribution of the motor can be obtained by employing the finite element method (FEM). The electromagnetic force and road excitation are input into differential equations to calculate the system response.

In the experiment, the revolving speed of the electric motor in stable operation was 1200 r/min. The excitation force of the electric motor was calculated as 15.6 kN by employing the FEM software ANSOFT. The equation shows that the excitation frequency is approximately 120 Hz. The frequency in other segments can be similarly estimated.

式中：$\mu_o$—空气中的磁导率，$\hat{n}$—沿表面 S 法方向上的单位矢量，$\boldsymbol{H_x}$和 $\boldsymbol{H_y}$分别为受力物体表面 S 上 x 和 y 方向上的磁场强度。电动机各处磁场分布可以通过有限元方法求得。将得到的电磁力与路面激励带入整个系统微分方程组求解系统响应。

所研究的分布式电驱动农用汽车试验电机稳定段运行转速为 1200r/min。电动机激振力可通过有限元软件 Ansoft 分析得出，激振力大小为 15.6kN，带入公式（3）可知激振力频率约为 120Hz。不同段频率可依此估计。

***Establishment of a three-dimensional vibration model***

To control the torque of the in-wheel drive motor and monitor the revolving speed of the wheel, a dynamic model of a distributed electric-drive agricultural vehicle that can be used to analyze the force between the vehicle and ground surface was constructed. Three DOFs in the vertical, horizontal and transverse directions were adopted for the whole vehicle.

The following preconditions were proposed to be taken into consideration for the dynamic model [13].

(1) The vehicle speed is less than 30 km/h; thus, the unbalanced excitations of tires and transmission shaft

***三维整机振动模型建立***

建立整车动力学模型来分析车辆与地面的作用力关系，达到控制轮边牵引电机转矩和监测电机转速的目的。选取纵向、侧向和横摆三个自由度，建立整车动力学模型。

从研究问题的需要出发，针对所研究的分布式电驱动农

can be ignored;

(2) The frame stiffness is sufficiently high, so the vibration generated by elastic deformation of the frame is ignored;

(3) The articulated body has no effect on the vertical vibration of the vehicle, and the DOF of steering is ignored;

(4) The non-suspended load is simplified as having a single DOF. Only the vertical DOF is considered in this model because it is significantly more influential than other DOFs of the load;

(5) Under the excitation of the engine, wheel electric motor and ground, the vibrations are only slightly near the equilibrium position. Therefore, the linear vibration of the vehicle bar centered on the horizontal plane and the angular vibration of the vehicle around the z-axis can be ignored.

Under these preconditions, an 11-DOF model of an agricultural vehicle is built as shown in Fig 1. In the figure, the front suspension is a hydro-pneumatic suspended structure and the rear suspension is a balanced beam structure. The vertical vibration, because of its effect on riding comfort, is the only factor considered for the engine vibration and drive motor vibration. The excitations from the road roughness, engine vibration and drive-motor vibration are considered. The vertical, roll and pitch DOFs of the engine are also introduced to reflect the effects of the stiffness and damping of the four mounts at the front and rear of the engine.

The 11 DOFs are listed as follows:

$Z_a$—barycentre displacement of the sprung mass in the vertical direction;

$A$—displacement of the pitch angle of the vehicle sprung mass around the bary centre;

$\theta_1$ and $\theta_2$—roll angular displacements of front and rear frames, respectively;

$Z_e$—engine displacement in the vertical direction;

$\alpha_e$—pitch angular displacement around the barycentre;

$\theta_e$—engine roll angle displacement around the centre of mass of the engine;

$Z_1$ and $Z_2$—displacements of the vehicle's front wheels in the vertical direction;

$\beta_1$ and $\beta_2$—angular displacements of the rear suspensions ;

Other parameters in the model are described as follows. $Z_{11}$–$Z_{61}$—the input displacements of the road that act on the six wheels, $F_{d1}$–$F_{d6}$—the input forces given by the vibrations of the six drive motors, $F_{de}$—the input force arising from engine vibration, $Z_1$ and $Z_2$—the vertical displacements of the hydro-pneumatic springs, $Z_3$–$Z_6$—the vertical displacements of middle- and rear-axle tires, $K_1$ and $K_2$—the stiffness coefficients of the hydro-pneumatic springs, $K_7$–$K_{12}$—the stiffness coefficients of the tires, $C_1$ and $C_2$—the damping coefficients of the hydro-pneumatic springs, $C_7$–$C_{12}$—the damping coefficients of the tires, $L_1$—the horizontal distance between a front wheel and the vehicle centre of mass, $L_2$ —the distance between a middle wheel and the centre of mass, $L_3$—the distance between middle and rear wheels, $L_4$—the distance between front wheels, $L_5$—the distance between rear wheels, $L_6$—the horizontal distance between the cab and the vehicle's centre of mass, $L_8$—the distance between the rear

用汽车的特点提出以下前提[13]：

（1）在低速情况下工作，故忽略轮胎和传动轴不平衡的激励；

（2）机身和车架刚度很大，忽略车身弹性引起的振动；

（3）铰接体对机身的垂直振动没有影响，不考虑铰接体转向自由度；

（4）非悬挂质量简化为单自由度质量系统，只考虑对整机振动影响较大垂向振动自由度；

（5）在发动机、轮边电机以及路面激励作用下，整车在平衡位置附近作微幅振动，车身质心在水平面内的振动忽略不计，机身绕 Z 轴的角振动忽略不计。

本文将车辆简化为 11 自由度三维整机模型（如图 1）。图中，前悬架为油气悬架，后悬架为平衡梁结构。影响乘坐舒适性的唯一因素是由发动机振动和电机振动引起的垂向振动。模型考虑了路面不平度激励，发动机振动和轮边驱动电机振动。发动机前后悬置的刚度和阻尼由发动机的垂向、侧倾以及俯仰三个自由度来描述。

模型 11 个自由度分别为：

$Z_a$ —整车簧载质量质心垂直方向位移；

$A$ —整车簧载质量绕质心的俯仰角位移；

$\theta_1$、$\theta_2$ —前后车体分别绕前后车体质心的侧倾角位移

$Z_e$ —发动机垂直方向位移；

$\alpha_e$ —发动机绕其质心的俯仰角位移；

$\theta_e$ —发动机绕其质心的侧倾角位移；

$Z_1$、$Z_2$ —前轮垂直方向位移；

$\beta_1$、$\beta_2$ —两平衡梁绕铰接处的角位移；

模型中其他参数如下：$Z_{11}$~$Z_{61}$—路面对六轮的输入位移；$F_{d1}$~$F_{d6}$—六个电机振动的输入力；$F_{de}$—发动机振动的输入力；$Z_1$、$Z_2$—油气弹簧与簧载质量连接点处的垂直位移；$Z_3$~$Z_6$—中后桥轮胎中心处的垂直位移；$K_1$、$K_2$—油气弹簧的刚度系数；$K_7$~$K_{12}$—轮胎的刚度系数；$C_1$、$C_2$—油气弹簧的阻尼系数；$C_7$~$C_{12}$—轮胎的阻尼系数；$L_1$—前轮距整机质心的水平距离；$L_2$—中轮到质心的水平距离；$L_3$—中后轮间的水平距离；$L_4$—前轮距；$L_5$—后轮距；$L_6$—驾驶室质心距整机质心的水平距离；$L_8$—发动机

engine and barycentre of the cab, $L_9$—the length of engine, $L_f$—the distance between front suspensions, $L_r$—the distance between rear suspensions, $M_0$—the sprung mass of the vehicle, $M_{01}$ and $M_{02}$—the sprung masses of front and rear frames respectively, $M_1$–$M_6$—the unsprung masses of the six wheels, $M_e$—the engine mass, and $I_1$—the longitudinal moment of inertia of the sprung mass that turns around the vehicle centre of mass. $I_2$—the horizontal inertia moment of the sprung load of the front frame, $I_3$—the horizontal inertia moment of the sprung load of the rear frame, $I_{e1}$—the inertia moment produced by the rotation of the engine around its longitudinal axis, and $I_{e2}$—inertia moment produced by the rotation of the engine around its horizontal axis.

尾部距驾驶室质心距离；$L_9$—发动机长度；$L_f$—发动机前悬之间的距离；$L_r$—发动机后悬之间的距离；$M_0$—整车簧载质量；$M_{01}$、$M_{02}$—前后车体簧载质量；$M_1$~$M_6$—六个车轮的非簧载质量；$M_e$—发动机质量；$I_1$—整车簧载质量绕质心纵向转动惯量；$I_2$—前车体簧载质量横向转动惯量；$I_3$—后车体簧载质量横向转动惯量；$I_{e1}$—发动机绕其质心纵向转动惯量；$I_{e2}$—发动机绕其质心横向转动惯量。

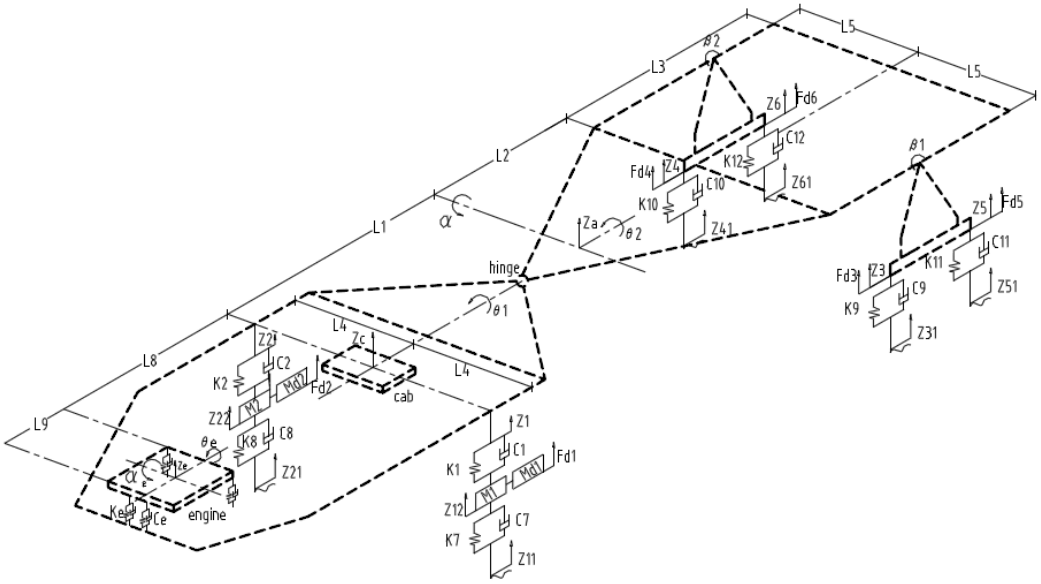


**Fig.1-** Model of an agricultural vehicle with 11 DOFs

The equations that govern the micro-vibration of the machinery are:

整机微分振动的动力学方程如下：

$$\begin{aligned}M_0\ddot{Z}_a &= C_1(\dot{Z}_{12}-\dot{Z}_1)+K_1(Z_{12}-Z_1)+C_2(\dot{Z}_{22}-\dot{Z}_2)+K_2(Z_{22}-Z_2)+C_{11}(\dot{Z}_{31}-\dot{Z}_3)+K_{11}(Z_{31}-Z_3)\\&+C_{12}(\dot{Z}_{41}-\dot{Z}_4)+K_{12}(Z_{41}-Z_4)+C_{13}(\dot{Z}_{51}-\dot{Z}_5)+K_{13}(Z_{51}-Z_5)+C_{14}(\dot{Z}_{61}-\dot{Z}_6)+K_{14}(Z_{61}-Z_6)\\&-K_e(Z_{e5}+Z_{e6}+Z_{e7}+Z_{e8})-C_e(\dot{Z}_{e5}+\dot{Z}_{e6}+\dot{Z}_{e7}+\dot{Z}_{e8})+F_{d1}+F_{d2}+F_{d3}+F_{d4}+F_{d5}+F_{d6}\end{aligned} \quad (8)$$

$$\begin{aligned}I_1\ddot{a} &= (L_2+L_3/2)[C_{11}(\dot{Z}_{31}-\dot{Z}_3)+K_{11}(Z_{52}-Z_5)+C_{12}(\dot{Z}_{41}-\dot{Z}_4)+K_{12}(Z_{51}-Z_5)+C_{13}(\dot{Z}_{51}-\dot{Z}_5)\\&+K_{13}(Z_{51}-Z_5)+C_{14}(\dot{Z}_{61}-\dot{Z}_6)+K_{14}(Z_{61}-Z_6)+F_{d3}+F_{d4}+F_{d5}+F_{d6}]-L_1[C_1(\dot{Z}_{12}-\dot{Z}_1)\\&+K_1(Z_{12}-Z_1)+C_2(\dot{Z}_{22}-\dot{Z}_2)+K_2(Z_{22}-Z_2)+F_{d1}+F_{d2}]-K_e[(Z_{e7}+Z_{e8})(L_1+L_8)\\&+(Z_{e5}+Z_{e6})(L_1+L_8+L_9)]-C_e[(\dot{Z}_{e7}+\dot{Z}_{e8})(L_1+L_8)+(\dot{Z}_{e5}+\dot{Z}_{e6})(L_1+L_8+L_9)]\end{aligned} \quad (9)$$

$$I_2\ddot{q}_1 = L_4[C_1(\dot{Z}_{12}-\dot{Z}_1)+K_1(Z_{12}-Z_1)-C_2(\dot{Z}_{22}-\dot{Z}_2)-K_2(Z_{22}-Z_2)]+I_{e2}\ddot{q}_e \quad (10)$$

$$\begin{aligned}I_3\ddot{\theta}_2 &= L_5[C_{11}(\dot{Z}_{31}-\dot{Z}_3)+K_{11}(Z_{31}-Z_3)+C_{13}(\dot{Z}_{51}-\dot{Z}_5)+K_{13}(Z_{51}-Z_5)+F_{d3}+F_{d5}\\&-C_{12}(\dot{Z}_{41}-\dot{Z}_4)-K_{12}(Z_{41}-Z_4)-C_{14}(\dot{Z}_{61}-\dot{Z}_6)-K_{14}(Z_{61}-Z_6)-F_{d4}-F_{d6}]\end{aligned} \quad (11)$$

$$M_1\ddot{Z}_{12} = C_7(\dot{Z}_{11}-\dot{Z}_{12})+K_7(Z_{11}-Z_{12})+C_1(\dot{Z}_1-\dot{Z}_{12})+K_1(Z_1-Z_{12})+F_{d1} \quad (12)$$

$$M_2\ddot{Z}_{22} = C_8(\dot{Z}_{21}-\dot{Z}_{22})+K_8(Z_{21}-Z_{22})+C_2(\dot{Z}_2-\dot{Z}_{22})+K_2(Z_2-Z_{22})+F_{d2} \quad (13)$$

$$I_4\ddot{b}_1 = L_3/2\cdot[C_{13}(\dot{Z}_{51}-\dot{Z}_5)+K_{13}(Z_{51}-Z_5)+F_{d5}-C_{11}(\dot{Z}_{31}-\dot{Z}_3)-K_{11}(Z_{31}-Z_3)-F_{d3}] \quad (14)$$

$$I_5\ddot{\beta}_2 = L_3/2\cdot[C_{14}(\dot{Z}_{61}-\dot{Z}_6)+K_{14}(Z_{61}-Z_6)+F_{d6}-C_{12}(\dot{Z}_{41}-\dot{Z}_4)-K_{12}(Z_{41}-Z_4)-F_{d4}] \quad (15)$$

$$M_e\ddot{Z}_e = K_e(Z_{e5}+Z_{e6}+Z_{e7}+Z_{e8})+C_e(\dot{Z}_{e5}+\dot{Z}_{e6}+\dot{Z}_{e7}+\dot{Z}_{e8})+F_e \quad (16)$$

$$I_{e1}\ddot{\alpha}_e = [K_e(-Z_{e5}-Z_{e6}+Z_{e7}+Z_{e8})+C_e(-\dot{Z}_{e5}-\dot{Z}_{e6}+\dot{Z}_{e7}+\dot{Z}_{e8})]\cdot L_9/2 \quad (17)$$

$$I_{e2}\ddot{\theta}_e = K_e[(Z_{e7}-Z_{e8})L_r+(Z_{e5}-Z_{e6})L_f]+C_e[(\dot{Z}_{e7}-\dot{Z}_{e8})L_r+(\dot{Z}_{e5}-\dot{Z}_{e6})L_f] \quad (18)$$

In the preceding equations, $Z_{e5}$–$Z_{e8}$ are the engine mount vertical displacements. The following dynamic equation can be obtained by solving the preceding equations:

其中：$Z_{e5}$~$Z_{e8}$ 为发动机微幅振动是发动机悬置垂向位移。联立上述方程可以解出整机的动力学方程：

$$M\ddot{Y}+C\dot{Y}+KY = K_t Q+C_t\dot{Q}+A_d F_d+A_e F_e \quad (19)$$

Where, ***M***—an 11 × 11 mass matrix, ***C***—an 11 × 11 stiffness matrix, ***K***—an 11 × 11 damping matrix, $C_t$—an 11 × 6 stiffness matrix of the tires, $K_t$—an 11 × 6 damping matrix of the tires, $A_d$—the drive motor excitation coefficient matrix, $A_e$—the excitation coefficient matrix of the engine, ***Q***—the excitation matrix of the ground surface, $F_d$—the excitation matrix of the drive motor, and $F_e$—the excitation matrix of the engine. These matrices are expressed as:

其中，***M***—11×11 阶质量矩阵；***C***、***K***—11×11 阶阻尼矩阵和刚度矩阵；***Ct*** 和 ***Kt***—11×6 阶轮胎阻尼矩阵和轮胎刚度矩阵；$A_d$—电机激励系数矩阵；$A_e$—发动机激励系数矩阵；***Q***—路面激励矩阵；$F_d$—电机激励矩阵；$F_e$—发动机激励。各矩阵表示为以下形式：

$$\mathbf{Y}=[Z_a \quad \alpha \quad \theta_1 \quad \theta_2 \quad Z_{12} \quad Z_{22} \quad \beta_1 \quad \beta_2 \quad Z_e \quad \alpha_e \quad \theta_e]^T, \qquad \mathbf{Q}=[Z_{11} \quad Z_{21} \quad Z_{31} \quad Z_{41} \quad Z_{51} \quad Z_{61}]^T$$

$$\mathbf{F_d}=[F_{d1} \quad F_{d2} \quad F_{d3} \quad F_{d4} \quad F_{d5} \quad F_{d6}]^T, \qquad \mathbf{A_e}=[0 \quad 0 \quad 0 \quad 0 \quad 0 \quad 0 \quad 0 \quad 0 \quad 1 \quad 0 \quad 0]^T$$

$$\mathbf{A_d}=\begin{pmatrix} 0 & 0 & 1 & 1 & 1 & 1 \\ 0 & 0 & L_2+L_7 & L_2+L_7 & L_2+L_7 & L_2+L_7 \\ 0 & 0 & 0 & 0 & 0 & 0 \\ 0 & 0 & L_5 & -L_5 & L_5 & -L_5 \\ 1 & 0 & 0 & 0 & 0 & 0 \\ 0 & 1 & 0 & 0 & 0 & 0 \\ 0 & 0 & -L_7 & 0 & L_7 & 0 \\ 0 & 0 & 0 & -L_7 & 0 & L_7 \\ 0 & 0 & 0 & 0 & 0 & 0 \\ 0 & 0 & 0 & 0 & 0 & 0 \\ 0 & 0 & 0 & 0 & 0 & 0 \end{pmatrix} \quad \mathbf{C_t}=\begin{pmatrix} 0 & 0 & C_9 & C_{10} & C_{11} & C_{12} \\ 0 & 0 & C_9(L_2+L_7) & C_{10}(L_2+L_7) & C_{11}(L_2+L_7) & C_{12}(L_2+L_7) \\ 0 & 0 & 0 & 0 & 0 & 0 \\ 0 & 0 & C_9L_5 & -C_{10}L_5 & C_{11}L_5 & -C_{12}L_5 \\ C_7 & 0 & 0 & 0 & 0 & 0 \\ 0 & Cs & 0 & 0 & 0 & 0 \\ 0 & 0 & -C_9L_7 & 0 & C_{11}L_7 & 0 \\ 0 & 0 & 0 & -C_{10}L_7 & 0 & C_{12}L_7 \\ 0 & 0 & 0 & 0 & 0 & 0 \\ 0 & 0 & 0 & 0 & 0 & 0 \\ 0 & 0 & 0 & 0 & 0 & 0 \end{pmatrix}$$

$$\mathbf{M}=\begin{pmatrix} M_0 & 0 & 0 & 0 & 0 & 0 & 0 & 0 & 0 & 0 & 0 \\ 0 & I_1 & 0 & 0 & 0 & 0 & 0 & 0 & 0 & 0 & 0 \\ 0 & 0 & I_2 & 0 & 0 & 0 & 0 & 0 & 0 & 0 & 0 \\ 0 & 0 & 0 & I_3 & 0 & 0 & 0 & 0 & 0 & 0 & 0 \\ 0 & 0 & 0 & 0 & M_1 & 0 & 0 & 0 & 0 & 0 & 0 \\ 0 & 0 & 0 & 0 & 0 & M_2 & 0 & 0 & 0 & 0 & 0 \\ 0 & 0 & 0 & 0 & 0 & 0 & I_4 & 0 & 0 & 0 & 0 \\ 0 & 0 & 0 & 0 & 0 & 0 & 0 & I_5 & 0 & 0 & 0 \\ 0 & 0 & 0 & 0 & 0 & 0 & 0 & 0 & M_e & 0 & 0 \\ 0 & 0 & 0 & 0 & 0 & 0 & 0 & 0 & 0 & I_{e1} & 0 \\ 0 & 0 & 0 & 0 & 0 & 0 & 0 & 0 & 0 & 0 & I_{e2} \end{pmatrix} \quad K_t=\begin{pmatrix} 0 & 0 & K_9 & K_{10} & K_{11} & K_{12} \\ 0 & 0 & K_9(L_2+L_7) & K_{10}(L_2+L_7) & K_{11}(L_2+L_7) & K_{12}(L_2+L_7) \\ 0 & 0 & 0 & 0 & 0 & 0 \\ 0 & 0 & K_9L_5 & -K_{10}L_5 & K_{11}L_5 & -K_{12}L_5 \\ K_7 & 0 & 0 & 0 & 0 & 0 \\ 0 & Ks & 0 & 0 & 0 & 0 \\ 0 & 0 & -K_9L_7 & 0 & K_{11}L_7 & 0 \\ 0 & 0 & 0 & -K_{10}L_7 & 0 & K_{12}L_7 \\ 0 & 0 & 0 & 0 & 0 & 0 \\ 0 & 0 & 0 & 0 & 0 & 0 \\ 0 & 0 & 0 & 0 & 0 & 0 \end{pmatrix}$$

The analytic solution can be obtained by putting the experimental parameters into the above equations. Given that road roughness is an important excitation for

根据上述方程组，可带入实车参数进行求解析解。另外路面不平度是设备行驶时最主要的激励，在进行汽车平顺

a moving vehicle, the input model of road excitation with accurate road information must be built before the vehicle riding comfort simulation and performance assessment is conducted. The road excitation is built by employing harmonic superposition as [19]:

性仿真研究和性能评价时，要获得足够准确的路面信息，建立路面激励的输入模型。本文用谐波叠加法建立路面输入模型。分别将每个小区间的正弦波叠加，即可得到用谐波叠加法模拟道路的时域模型，如下所示[19]：

$$q(t)=\sum_{i=1}^{n}\sqrt{2S_q(n_{mid-i})\Delta n_i}\sin(2\pi n_{mid-i}ut+\theta_i) \quad (20)$$

Where, $\theta_i$ is an independent random variable distributed uniformly in the range of 0 to 2π, $S_q(n)$ is the power spectral density (PSD) of the road roughness, and the spatial frequency n ranges from $n_1$ to $n_2$ ($n_1$ = 0.011 $m^{-1}$, $n_2$ = 2.83 $m^{-1}$). The spatial frequency $n$ is divided into multiple intervals between $n_1$ and $n_2$, and the centre frequency of each interval is expressed as $n_{mid-i}$ ($i$ = 1, 2,…, $n$).

The random displacement of the road at the front left wheel $q_1(t)$ and that at the front right wheel $q_2(t)$ can be determined by assigning corresponding values to $\theta_i$ The random displacements of the road at the rear wheels can be deduced from those of the front wheels according to a time delay as:

式中，$\theta_i$ 为[0,2π]上均匀分布的相互独立的随机变量。其中 $S_q$（$n$）为路面不平度 PSD，空间频率范围为 $n_1$< $n$< $n_2$($n_1$=0.011$m^{-1}$, $n_2$=2.83$m^{-1}$)。将 $n_1$< $n$< $n_2$ 的空间频率区间划分为 $n$ 个小区间，设 $n_{mid-i}$($i$=1,2,…,$n$)为每个小区间的中心频率。

在上式中 $\theta_i$取不同值可以得出左前轮和右前轮的路面随机位移输入 $q_1$（$t$）、$q_2$（$t$），左中后轮和右中后轮可由时间延迟得出：

$$q_3(t)=q_1(t+(L_1+L_2)/u),\ q_5(t)=q_1(t+(L_1+L_2+L_3)/u),$$

$$q_4(t)=q_2(t+(L_1+L_2)/u),\ q_6(t)=q_2(t+(L_1+L_2+L_3)/u),$$

According to the Chinese National Standard GB7031-1986, roads are classified into eight levels based on road roughness. The road condition in the experiment corresponds to the standard level D. Employing harmonic superposition, the excitation of the road roughness on the left and right of the travelling vehicle at a speed of 30 km/h is simulated (see Fig. 2 for the excitation of the front left wheel of the vehicle).

In a test conducted to verify the coupled vibration model, a vehicle travelled along a random road on which two pieces of wood were placed. Figure 3 shows the road roughness excitation when the machinery travelled at 10 km/h on the B grade standard pavement.

国标 GB7031-1986 根据路面不平度系数 $G_q(n_0)$的大小，将路面分为 8 级，试验路面情况一般，应选用较为平整但碎石较多的 D 级路面模型建模。本文用谐波叠加法编写了速度为 30km/h D 级标准路面得到车辆实际行驶过程中左右车辙的路面不平度激励如图 2 所示。

在随机路面的基础上加入两个高度分别为 $H_1$、$H_2$ 的木块，其宽度分别为 $b_1$、$b_2$，间距为 $S_1$，仿真时车辆以速度 $v$ 均速驶过木块。图 3 为速度为 10km/h，B 级标准路面下得到车辆实际行驶过程中左右车辙的路面不平度激励。

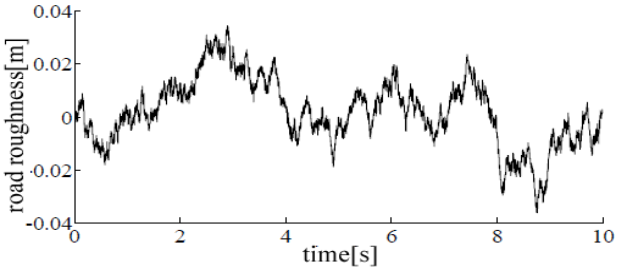


**Fig.2-** Road excitation of machinery's front left wheel

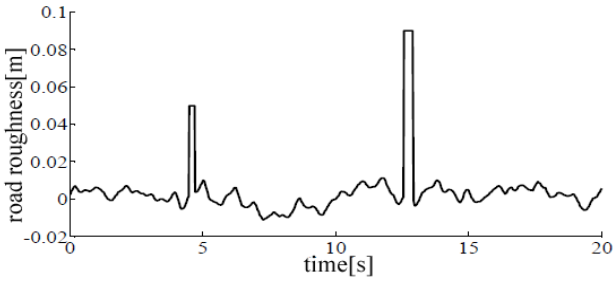


**Fig.3-** Simulation of road roughness

## RESULTS

### *Simulation results*

A simulation of an idling machinery moving at a speed of 30 km/h on a road corresponding to ISO level D was performed. The coupled vibration was simulated by inputting the structural parameters, excitation of random roads, engine excitation and drive-motor

## 结果

### *耦合振动仿真分析*

将模型各参数数值、路面随机激励、发动机与电机激励理论值代入模型中可得仿真结。这里，以空载情况下速度 30km/h，ISO D 级路面为例进行分析。图 4 表示仿真分

excitation into the model established in the previous section. A time-domain plot and the PSD of the vertical vibration of the cab are shown in Figs. 4 and 5 respectively. For comparison, the results obtained when ignoring the excitations of the engine and drive motor are also shown.

The simulation started from a static state. Figure 4 reveals that the maximum acceleration is 2.5 m/s$^2$ when the excitations of the engine and drive motor are included. After 1 s, a state of stable vibration is reached regardless of whether the excitations of the engine and drive motor are included or not. The maximum acceleration is 0.5 m/s$^2$ when the excitations of the engine and drive motor vibration are included, whereas it is only 0.4 m/s$^2$ when the excitations are excluded. The trend is seen more clearly when the result is converted to the frequency domain by Fourier transformation as shown in Fig 5.

析后驾驶室垂向振动加速度时域图，图 5 为驾驶室垂向振动加速度功率谱密度，进行了耦合振动模型仿真，及忽略电动机与发动机振动影响下的仿真。

图 4 仿真是从静止状态开始的，可以看出在考虑发动机和电机振动激励的条件下，最大加速度可以达到 2.5 m/s$^2$，在 1s 后二者都进入平稳振动阶段，平稳振动阶段耦合振动模型加速度峰值为 0.5 m/s$^2$ 左右，而在忽略发动机和电动机振动的仿真模型结果中，平稳阶段振动加速约为 0.4 m/s$^2$。为了便于分析，通过傅里叶变换得到频域图如图 5 所示。

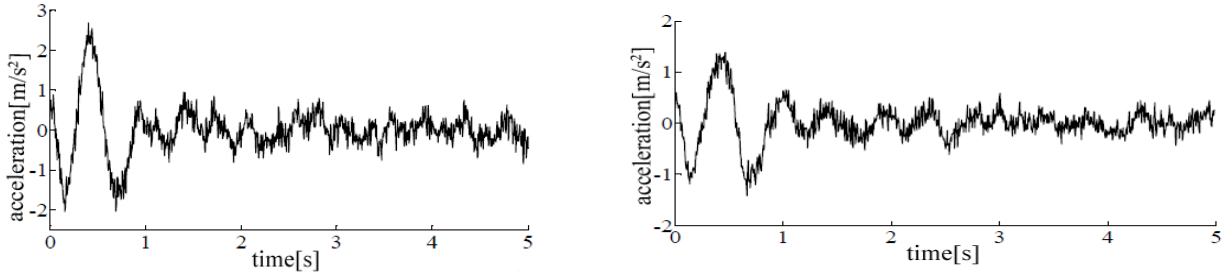


(a) Including the vibration of the engine and drive motor (b). Excluding the vibration of the engine and drive motor

**Fig.4 -** Vertical acceleration of the cab vibration

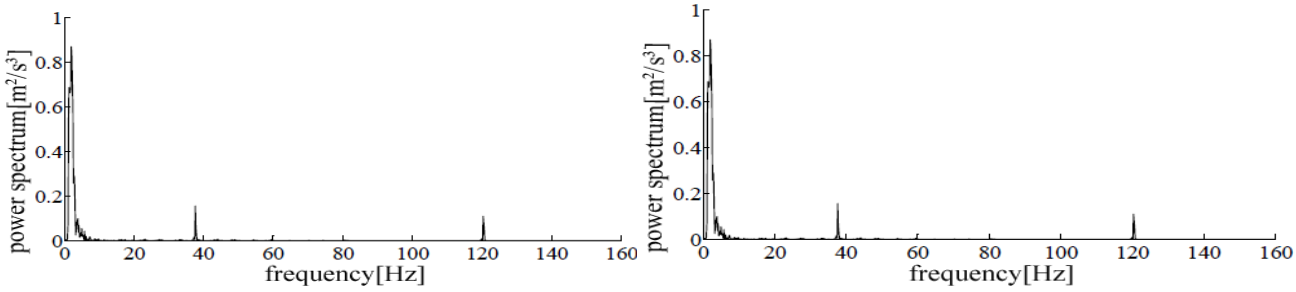


(a) Including the vibration of the engine and drive motor (b) Excluding the vibration of the engine and drive motor

**Fig.5 -** Vertical acceleration PSD of the cab vibration

The comparison of Fig. 5 (a) and (b) shows that the power at low frequency is affected by the engine and drive motor. The maximum power increases from 0.6 m$^2$/s$^3$ to 0.85 m$^2$/s$^3$ after the inclusion of the excitations from the engine and drive motor. Additionally, obvious spikes in the power spectrum appear at the frequency of the engine (37.5 Hz) and at the frequency of the drive motor (120 Hz). Significant power increases in the frequency domain analysis cannot be ignored.

***Experimental validation***

To validate the coupled vibration model, an experiment was conducted using an agricultural vehicle. The machinery was controlled by six-wheel-drive motors independently. Acceleration sensors were placed on fixed surfaces of the cab, the rear frame, the left

通过图 5 对比，总体可见耦合振动模型下驾驶低频段功率明显增加，其最大值为 0.85 m$^2$/s$^3$，远大于简化模型结果，忽略发动机及电动机振动模型得到的功率谱最大值只为 0.6 m$^2$/s$^3$，同时在发动机 37.5Hz 激振力处，电动机两倍供电频率 120Hz 处，在频域分析中存在明显功率，不可忽略。

***整车平顺性试验***

采用实车进行了实验以验证耦合振动模型，该车辆是由 6 个轮边驱动电机独立驱动。加速度传感器被安置在驾驶室的固定表面上，后车架以及前后悬架，如图 6 所示。通

suspension, the right suspension and a drive motor as shown in Fig. 6. The signals of vibration acceleration were measured using a data capture card. The signals of the engine and drive motor speeds were collected using a controller area network (CAN) bus device. Acceleration signals of motor vibration at low frequency were filtered to remove the vibration excitation of the road. The sampling frequency of each sensor was 2560 Hz, which was appropriate for signal analysis.

过采集卡采集传感器安装位置的振动加速度信号，通过 CAN 总线采集发动机以及电机转速信号，其中电机上方振动加速度数据需要进行滤波去掉低频段路面的振动激励。每个传感器的采样频率为适合数据分析的 2560Hz。

**Fig.6 -** Sensors placed on the vehicle

The experiment was conducted on a fine-gravel road corresponding to ISO level D. The vehicle was driven at an even speed of 30 km/h with relative error less than ±5%. The mean value was calculated for three repetitions of the experiment. The vertical vibration acceleration of the cab at the stage of stable running is shown in Fig. 7. Figure 8 presents the vertical vibration PSD after fast Fourier transformation. Fig 9 clearly shows the PSD of the drive motor at high frequency by focusing on the data range of 0–0.2 $m^2/s^3$.

设备的实验在相当于 ISO D 级的细砂石路面上进行，以 30km/h 速度匀速行驶，车速变化不大于±5%，且同一工况条件下的试验重复三次，结果取其平均值。平稳运行阶段实测驾驶室垂向振动加速度如图 7。经 FFT 变换后为图 8，即驾驶室垂向振动加速度功率谱密度，为了清晰展示高频段的电动机功率谱可截取 0~0.2 $m^2/s^3$ 段功率谱进行分析，得到图 9。

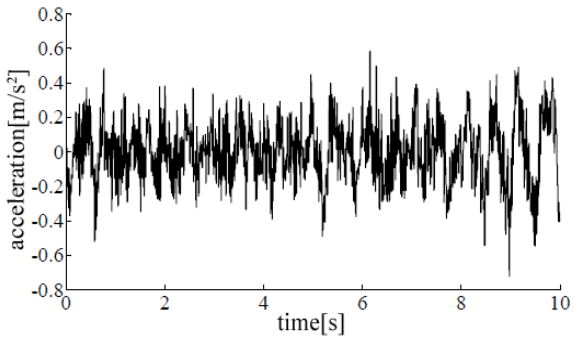


**Fig.7 -** Measured vertical vibration acceleration of the cab

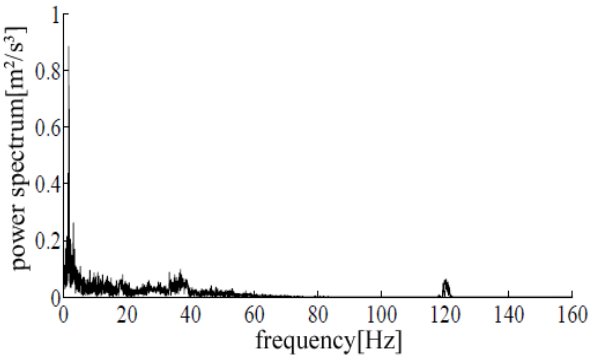


**Fig.8 -** PSD of the vertical vibration acceleration of the cab

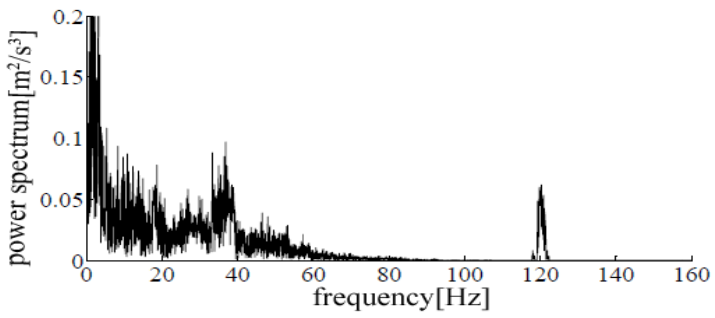


**Fig.9 -** PSD of the vertical vibration acceleration of the cab within 0–0.2 $m^2/s^3$

Comparison of the acceleration time-domain curves and PSD curves of the cab obtained in the experiment with the simulation results reveals that the coupled vibration model and experimental results are basically consistent. The power spectrum obtained in the experiment mainly ranged from 1 Hz to 20 Hz and had a peak value of 0.85 $m^2/s^3$ at 2 Hz. Additional peaks at the excitation position of the engine and drive motor were found in both simulation and experiment. Figure 9 shows that the PSD had a second peak of 0.06 $m^2/s^3$ near the excitation frequency of the drive motor, 120 Hz. Another obvious peak value of 0.09 $m^2/s^3$ was recorded at a frequency of approximately 37 Hz. The result obtained excluding the vibrations of the engine and drive motors showed a peak value of only 0.6 $m^2/s^3$, which was obviously lower than the value when these two vibrations were included. The good match of simulation and experimental results shows that the multisystem coupled vibration model including the excitations of the engine and drive motors can be used to simulate the vibrations and riding comfort of the cab.

We next consider the vehicle running at a speed of 10 km/h over two blocks with heights of 0.06 m and 0.09 m and spaced 10 m. Table 1 provides the root mean square of the vibration acceleration in both simulation and experiment.

将试验得出驾驶室的振动加速度时域曲线以及功率谱密度曲线与三维整车模型得出仿真结果作比较，耦合振动模型与实测模型加速度功率谱基本一致，主要出现在低频段 1-20hz 以内，在 2Hz 左右出现约为 0.85 $m^2/s^3$ 的峰值，在发动机和电动机激振频率处都有明显峰值。图 9 表明在高频段电动机激励力频率 120 Hz 附近驾驶室出现第二个峰值，驾驶室峰值大小为 0.06 $m^2/s^3$，在 37Hz 左右还有一个明显峰值，大小为 0.09 $m^2/s^3$。而忽略了电动机和发动机的模型结果，在低频段整体峰值较低，最高值只有 0.6 $m^2/s^3$，且在别处再无明显峰值出现。仿真和实验结果基本保持一致表明包括发动机和驱动电机激励的多系统耦合振动模型可用于模拟驾驶室的振动和行驶舒适性。

接下来考虑车辆以 10km/h 通过在两个高为 0.06m 和 0.09m 木块的情况。表一给出了在仿真和实验时振动加速度的均方根。

**Table 1**

**Root mean square of vibration acceleration under pulse excitation (m/s)**

| Measuring point | Test value | Simulation value |
|---|---|---|
| Cab | 0.2801 | 0.2967 |
| Upper fulcrum of the left suspension | 0.3124 | 0.3019 |
| Rear frame | 0.4933 | 0.5123 |
| Upper fulcrum of the left motor | 0.7123 | 0.7506 |

The acceleration results obtained under the impulse excitation are similar to those obtained for the random road. The experimental acceleration (Fig. 11) differs from the simulation acceleration (Fig. 10) by only less than 10%, and the trends of the acceleration are consistent between simulation and experiment.

在脉冲激励下获得的加速度结果与在随机路面上获得的结果类似。实验加速度（图 11）略小于仿真加速度（图 10），但不超过 10%。实验和仿真加速度的变化趋势是一致的。

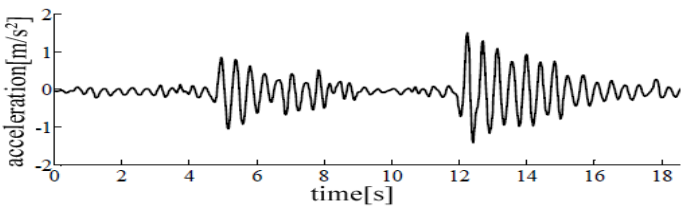


**Fig.10 -** Vibration acceleration in simulation

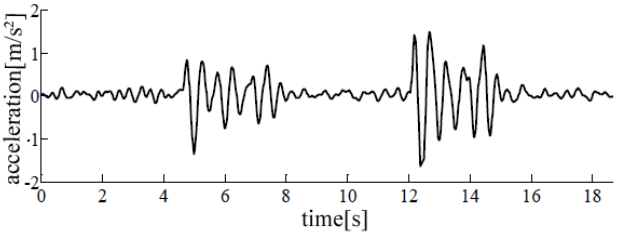


**Fig.11 -** Vibration acceleration in experiment

Fig 10 and Fig 11 reveal obvious fluctuations in acceleration near 4.5 s. The instantaneous acceleration reached 0.93 $m/s^2$ and 1.29 $m/s^2$ in the experiment and simulation, respectively. Then, under the effect of suspension damping, the acceleration began to attenuate. At 12 s, a second obvious fluctuation occurred, with the instantaneous acceleration reaching 1.41 $m/s^2$ in the experiment and 2.06 $m/s^2$ in the simulation. The acceleration then gradually decayed.

由图 10 和图 11 可以看出仿真与试验的加速度值均在 4.3s 附近第一次发生明显波动，试验瞬时加速度大小达到 0.93$m/s^2$，仿真瞬时加速度大小达到 1.29$m/s^2$，之后在悬架阻尼的作用下开始衰减，在 11s 时仿真与试验的加速度值出现第二次明显波动之后，试验瞬时加速度大小达到 1.41$m/s^2$，仿真瞬时加速度大小达到 2.06$m/s^2$，之后逐渐衰减并恢复正常。

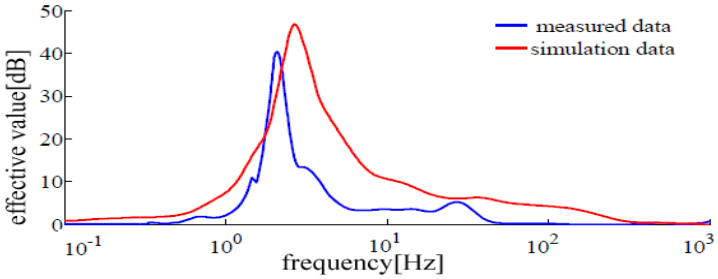


**Fig.12 -** Power spectrum of the vibration acceleration of the cab

Figure 12 shows the power spectra of the vibration acceleration of the cab in the experiment and simulation. The peak value is 40.26 dB at 1.75 Hz in the experiment and 46.1 dB at 1.98 Hz in the simulation, showing good agreement. Both power spectra are concentrated at low frequency within 1-5 Hz. Owing to the differences between the model and the real machinery, the acceleration of cab vibration is higher in the simulation than in the experiment, but the acceleration fluctuation time and trend of acceleration are roughly the same. The same results are observed in the frequency domain as in the time domain, further verifying the accuracy of the single-point contact model of a machinery.

## CONCLUSION

A model was constructed to analyze the vibration response of a distributed electric-drive agricultural vehicle considering coupled excitations of the road roughness, engine and drive motors. The conclusions are shown as follows:

(1) The experiment result shows that the 11-DOF vibration model built in consideration of the coupled excitations of the road can accurately describe the vibration characteristics of the distributed electric-drive agricultural vehicle.

(2) The excitation forces of the engine and drive motors increased the PSD of the vehicle acceleration, and obvious PSD peaks registered at the excitation frequency. Therefore, the excitation forces of the road roughness, drive motors and engine must all be considered to ensure the riding comfort and reliability of the distributed electric-drive agricultural vehicle.

Compared with the research on a passenger vehicle, that on the riding comfort of agricultural vehicle has obvious differences. Air suspension with variable stiffness can improve riding comfort and has a good application prospect in the field of agricultural vehicle.

## ACKNOWLEDGEMENT

This study was supported by the National High Technology Research Program (2011AA060404).

## REFERENCES

[1]. Ackermann, J Robust. (1993) –*Yaw damping of cars with front and rear wheel steering,* Transactions on Control Systems Technology, vol.1, no.1, pp.15-20;

[2]. Gao Yanlei, Zhou Yanpei, Sun Xiaoning. (2014) –*Engine Vibration Certification*, Procedia Engineering, vol.80, pp.1-9;

[3]. Gu Yu, Li Shaoxiong, Li Rui, Li Qiang. (2013) –*The numerical simulation and finite-element analysis of the motor vibration problem based on the base anchor softening layer, Advanced Materials Research*, vol.815, pp.860-867;

图 12 表示仿真和实验所得驾驶室振动加速度的功率谱密度。两种功率谱都集中在 1-5Hz 的低频范围内，实验加速度功率谱密度在 1.75Hz 出现最大值 40.26dB，仿真加速度功率谱密度在 1.98Hz 出现最大值 46.1dB，仿真数据与实验数据基本保持一致。由于所建模型与实车之间的差异，仿真的加速度值要高于比实验得到的加速度值，但是其波动时间和趋势基本一致。频域和时域分析得到了相同的结果，进一步验证了车辆单点接触模型的准确性。

## 结论

论文提出了考虑路面不平度和电动机、发动机耦合激振来分析实车系统振动响应的方法。分析了考虑耦合激振后系统响应的差别，主要结论如下：

(1)所建立电机激振力、发动机振动及路面激励的十一自由度整机三维振动系统模型经实车试验验证结果表明，该模型能够准确的反应分布式农用汽车的振动特性。

(2)电动机和发动机振动激励力会整体增大整机加速度功率谱，在激励力频率处会出现明显峰值，不可忽略。为提高电动车辆的平顺性及可靠性，需兼顾电机激振力和路面激励，耦合激励模型对农用机械的悬架及整车平顺性设计有指导意义。

农用机械的行驶平顺性研究与乘用车相比具有一定的差距，采用可变刚度的空气弹簧可提高整机的平顺性，是论文下一步研究的方向。

## 致谢

国家高技术研究发展计划(2011AA060404)。

## 参考文献

[1]. Ackermann, J Robust. (1993) –*前后轮转向时的侧偏阻力研究*. 控制系统技术学报, 第1卷, 第1期, 15-20;

[2]. 高艳蕾, 周艳培, 孙晓宁. (2014) –*发动机振动检测*, 能源工程, 第 80 卷, 1-9;

[3]. 谷雨, 李少雄, 李锐, 李强. (2013) –*基于基础垫软化层的电机垂向振动问题的数值模型和有限元分析*, 先进材料研究, 第815期, 860-867;

[4]. Hu Baoyang, Zhang Qiang, Li Qiangqiang.(2013) –*Analysis of Coach Vibration Based on Engine Excitation*. Agricultural Equipment and Vehicle Engineering. vol.51, no.4, pp30-34,
[5]. Liu Weixin. (2001) –*The Automobile Design*. Beijing: Tsinghua University Press;
[6]. Li Chaofeng, Wang Degang. (2009) –*Study and Application of 11-DOF Nonlinear Riding comfort Model for Vehicle.* Journal of Northeastern University, vol.30, no.6, pp.857-861;
[7]. M Canale, L Fagiano, M Milanese. (2007) –*Robust vehicle yaw control using an active differential and IMC techniques*. Control Engineering Practice, vol.21, no.15, pp.923-941;
[8]. Meng Fanwei, Liu Chengying, Li Zhijun, Wang Liping. (2013) –Linear motor vib*ration suppression using current oversampling, Qinghua Daxue Xuebao, vol.53, no.3, pp.307-312;*
[9]. Perez, Pinal F, CervantesI, Emadi A. (2009) –*Stability of an Electric Differential for Traction Applications*, IEEE Transactions on Vehicular Technology, vol.58, no.7, pp.76-82;
[10]. Paulo Cezar, Jorge Nei Brito. (2013) –*Detection of Electrical Faults in Induction Motors Using Vibration Analysis*, Journal of Quality in Maintenance Engineering, vol.194, pp.85-92;
[11]. Song Jianqing. (2014) –*The Technology of Driving AC Servo Motor Based on FPGA, Shang Dong University,*
[12]. Tan Di. (2013) –*Dynamics and Structure Optimization of the In-wheel Motor System with Rubber Bushing*. South China University of Technology;
[13]. Umesh Kumar Rout, Rabindra Kumar Sahu, Sidhartha Panda. (2013) –*Design and Analysis of Differential Evolution Algorithm Based Automatic Generation Control for Interconnected Power Sys-tem,* Electric Engineering, vol.13, no.4, pp.409-421;
[14]. Wang Junnian, Wang Qingnian, Song Chuanxue. (2010) –*Co-simulation and Test of Differential Drive Assist Steering Control System for Four-wheel Electric Vehicle*. Transaction of the Chinese Society for Agricultural Machinery, vol.1, no.6, pp.8-13;
[15]. Wang Dengfeng, Li Wei, Chen Shuming. (2011) –*Transfer Path Analysis of Power Train Vibration on Vehicle Riding comfort,* Journal of Jilin University(Engineering and Technology Edition), vol.41, no.2, pp.92-98;
[16]. Wellman Thomas, Govindswamy Kiran. (2007) –*Aspects of driveline integration for optimized vehicle NVH characteristics,* SAE Technical Paper Series;
[17]. Yu Houyu, Huang Miaohua. (2011) –*Experimental Research of Electronic Differential Control for In-wheel Motor Drive Electric Vehicle*, Journal of Wuhan University of Technology, vol.33, no.5, pp.148-151;
[18]. Zhang Guangrong, Yu Dejie. (2010) –*Study on Automotive Interior Structural Noise Excited by Engine,* Vibration and Noise Control, vol.1 No.1, pp45-47,
[19]. Zhang Daisheng, Li Wei. (2002) –*Simulation for Slip Ratio of An Automobile Antilock-braking System Based on Fuzzy Logic Control Method*, Transaction of the Chinese Society for Agricultural Machinery, vol.33, no.2, pp.29-31,

[4]. **胡宝洋，张强，李锵强**.(2013)-***基于发动机激励的客车振动分析***. **农业装备与车辆工程**.**第51卷, 第4期**，30-34,
[5]. 刘惟信. (2001) –*汽车设计*. 北京: 清华大学出版社;
[6]. 李朝峰, 王得刚. (2009) –*11自由度非线性车辆平顺性模型的研究及应用*, 东北大学学报(自然科学版), 第06期, 857-860;
[7]. M Canale, L Fagiano, M Milanese. (2007) –*基于主动差速器和IMC技术的车身横摆控制*, 控制工程实践, 第21卷, 第15期, 923-941;
[8]. 孟凡伟, 刘成英, 李志军, 王丽萍. (2013) –*电流采样法对线性电机振动抑制*, 清华大学学报, 第53卷, 第3期, 307-312;
[9]. Perez, Pinal F, Cervantes I, Emadi A. (2009) –*电子差速器牵引稳定性研究*. IEEE车辆技术学报, 第58卷, 第7期, 76-82;
[10]. Paulo Cezar, Jorge Nei Brito. (2013) –*应用垂向振动分析感应电机的电气故障*, 质量维修工程日报, 第194期, 85-92;
[11]. 宋建庆.（2014）–*基于FPGA的交流伺服电机驱动技术*. 山东大学,
[12]. 谭迪. (2013) –*内置悬置的轮毂电机驱动系统动力学特性及结构优化*. 华南理工大学;
[13]. Umesh Kumar Rout, Rabindra Kumar Sahu, Sidhartha Panda. (2013) –*用于互联电力系统自动发电控制的差分进化算法的设计与分析*, 电子工程, 第4期, 409-421;
[14]. 王军年, 王庆年, 宋传学. (2010) –*四轮驱动电动汽车差动助力转向系统联合仿真与试验*, 农业机械学报, 第41卷, 第6期, 8-13;
[15]. 王登峰, 李未, 陈书明. (2011) –*动力总成振动对整车行驶平顺性的传递路径分析*, 吉林大学学报(工学版), 第S2期, 92-97;
[16]. Wellman Thomas, Govindswamy Kiran. (2007) –*基于 NVH 特性的车辆传动系统的集成优化*, SAE 技术论文系列;
[17]. 喻厚宇, 黄妙华. (2011) –*电动轮车电子差速控制的试验研究*, 武汉理工大学学报, 第33卷, 第5期, 148-151;
[18]. 张光荣,于德介.(2010) –*发动机激励引起的车内结构噪声研究*, 噪声与振动控制, 第1卷, 第1期, 45-47,
[19]. 张代胜, 李伟. (2002) –*基于滑移率的汽车防抱模糊控制方法与仿真*, 农业机械学报, 第 33 卷, 第 2 期, 29-31.